Tau Aggregation is Altered by Variations in its Projection Domain

Kayleigh Mason-Chalmers, Aanzan Sachdeva, Gabryelle Kolk, Justin C. Touchon and Zachary J. Donhauser

Vassar College Department of Chemistry, 124 Raymond Ave Poughkeepsie, NY 12604

Key Words: tau, aggregation, R5L

Abstract:

The intrinsically disordered microtubule-associated protein tau is known for its aberrant aggregation into neurofibrillary tangles as found in neuropathologies such as Alzheimer's disease. This study compares three N-terminal isoforms of R5L and of wild type tau to investigate how this mutation and the length of the projection domain affects aggregation behavior. The total amount of polymerization was analyzed using a thioflavin S assay where tau aggregation is induced using arachidonic acid *in vitro*. Tau polymers were also analyzed using atomic force microscopy imaging to compare tau filament lengths and morphologies. We observed that the R5L mutation has a greater impact on filament length in shorter N-terminal isoforms of tau, whereas in longer N-terminal isoforms the mutation impacts the total amount of tau aggregation. These observations suggest that the R5L mutation affects the kinetic nucleation-elongation pathway of tau fibrillization, where the mutant impacts nucleation in 2N and 1N isoforms, but has a more significant impact on elongation in the 0N isoform.

1. Introduction:

The microtubule associated protein tau is primarily found in axons both in the peripheral and central nervous system, where it has important roles in cellular organization, and where it assists in the assembly, stabilization and organization of microtubules.[1–5] Tau also has other lesser known functions such as influencing the localization of specific cellular kinases, interacting with the cellular membrane, and affecting the movement of motor proteins.[6–8] Tau is also widely known for its role in neurodegenerative disease,[4,5] aggregating into paired helical filaments (PHFs) and straight filaments (SFs) which largely comprise neurofibrillary tangles (NFTs), structures that are highly correlated with the class of diseases known as tauopathies. These diseases include Alzheimer's disease (AD), frontotemporal dementia (FTD), and Pick's disease,[2,3,9–11] where aggregates and NFTs are correlated with neuronal dysfunction and death that may cause or further the progression of diseases.[1] Loss of tau native function and the related disruption of microtubule networks may be contributing factors to disease.[3] In advanced AD patients, pathological tau filaments have been found to completely overwhelm and replace microtubules in dendrites.[12]

The tau protein consists of four major regions (depicted in Figure 1a): the N-terminus (or projection domain, PD), the proline-rich region (PRR), the microtubule-binding domain (MTBD), and the C-terminus.[2,7] The projection domain, which is of key interest in this paper, is highly negatively charged and projects off of the surface of microtubules when tau is bound to these structures. In comparison, the highly positively charged MTBD binds to the negatively charged surface of microtubules. This interaction is largely driven by electrostatic interactions and supplemented by the positively charged PRR.[7,13–15] The short C-terminus is negatively

charged, and is thought to also project off of the microtubule surface.[2,5] As tau is highly charged, it does not form a singular stable secondary structure in solution,[16] and is acid- and heat-stable.[6]

Tau arises from one MAPT gene that is alternatively spliced into six major isoforms, which vary in the presence or absence of exons 2, 3, and 10. Exons 2 and 3 determine the number of N-terminal repeats (0,1, or 2, corresponding to 0N, 1N, and 2N tau), while the presence or absence of exon 10 results in tau with four (4R) or three (3R) MTBD repeats, respectively.[1,4] In humans, the naturally occurring distribution of tau is primarily composed of 0N and 1N tau, making up 37% and 54% of the population respectively, whereas 2N makes up 9%.[5] The ratio of 3R:4R tau may also be important, as it has been related to disease.[4,5] Tau isoforms with more N-terminal repeats have a higher negative charge in that region, which may impact the function of the projection domain. In the present work, only the N-terminal isoforms with all four MTBD repeats were investigated (Figure 1).

Numerous tau mutations have been found to decrease microtubule affinity, and most are found in the MTBD.[17,18] However, evidence shows that differences in the N-terminus' length and conformation affect aggregation from monomeric soluble tau into filamentous tau,[19,20] and physical and structural changes in the PD are key indications of dysfunctional tau.[20] Mutations in the projection domain such as R5L and R5H are relatively understudied, though they are related to diseases such as familial frontotemporal dementia (FTD) with parkinsonism in chromosome 17 (FTDP-17) and progressive supranuclear palsy (PSP),[17,18,21–23] R5L is specifically related to neuronal death in the substantia nigra and locus coeruleus in both FTDP-17 and PSP.[23] These mutated tau isoforms tend to impact the kinetics of aggregation,[23] and it is thought that related mutations cause lowered microtubule affinity, therefore allowing dissociation from microtubules followed by aggregation.[23] The connection of these particular mutations to disease highlight the

PD's relationship to aggregation and disease. The focus of the present work is the R5L mutant, which has an arginine to leucine point mutation in the fifth amino acid of tau, that can be used to further investigate the role of the N-terminus in the dynamics of tau aggregation.[17,18]

Previous work has shown that the R5L mutant affects the growth of plus ends of microtubules, increases the microtubule shrinkage rate *in vitro*, and causes a decrease in microtubule assembly, although it does not affect tau's interactions with tubulin.[24] The mutation disrupts the N-terminus/microtubule interactions and may disrupt tau-tau interactions, resulting in a lower patch density and frequency on microtubules as compared to wild type. The formation of these patches highly influence the physiological cargo transport on microtubules.[15]

Although tau is canonically an intrinsically disordered protein, there have been numerous studies indicating that it can adopt transient or loosely folded structures in solution, and that alterations in these structures may be related to tau pathologies. For example, Mandelkow and coworkers reported that tau adopts a dynamic "paperclip" conformation, where the ends of the protein fold in and the C-terminus interacts with both the MTBD and PD (Figure 2).[2,25–27] This hairpin structure has been found for both the longest (2N4R) and shortest (0N3R) tau. Previous studies have found that the R5L and MTBD mutations alter tau's ability to form this structure,[28–30] adopting more extended conformations[30] or affecting the interaction between the MTBD, N- and C-terminals.[28] Other secondary structures of tau have been identified such as the Alz50 epitope which has interactions between the MTBD and PD,[31] intermolecular β-sheets in the MTBD,[32] or α-helices.[33] When tau dissociates from microtubules, the protein fluctuates between its transient secondary structures.[25,30,34–36] Numerous studies have suggested that tau unfolding from its secondary structures into an extended conformation is required for the formation of tau filaments.[9,25,30,34–36]

Tau forms filaments under a nucleation-elongation model (Figure 2).[9,25,30] Monomeric extended tau first nucleates into a dimer which is initiated by the MTBD's ^{275}VQIINK^{280} and ^{306}VQIVYK^{311} that misfold into β-strands.[26,29] However, tau is known to misfold in numerous ways, and primary nucleation is dependent on the efficiency of tau misfolding into disease-specific dimers.[32] These dimers then undergo a secondary nucleation with other dimers to form a seed. Numerous aggregation studies have shown that either primary or secondary nucleation are rate-determining, with both being thermodynamically unfavorable.[9,26,29,32,35] After the seed reaches its critical size,[9,35,36] tau monomers are added unidirectionally to form elongated SFs or PHFs.[9,10,29,37–40] The process of elongation is the thermodynamic driving force of aggregation, yet is semi-reversible, as filaments can fragment into shorter fibers but will not disaggregate into tau's monomeric state.[16,41] Shorter fibers may also result from more rapid primary and secondary nucleations, while conversely if these steps are slow relative to elongation, longer fibers result.[35] Once adequately elongated, tau fibers can cluster via higher order interactions to form neurofibrillary tangles.[9]

The rate and extent of tau aggregation has been found to be influenced by the projection domain.[19] The presence of the N-terminus inhibits polymerization, and tau aggregates more readily when this region is eliminated.[30,42,43] The number of N-terminal repeats also influences aggregation, as 0N has been shown to form globular clusters rather than filaments,[23,44] and 1N forms 50% more fibers than 2N.[19,23] The lower acidity of shorter N-terminal tau isoforms are thought to increase the tendency of tau to form clusters.[44]

Tau filaments generally consist of a stable core comprised by hydrogen-bonded β-strands of the R3 and R4 repeats while the termini of the protein project off the core as a disordered "fuzzy coat."[36,45–48] The projection domain largely participates in the fuzzy coat, with some

evidence suggesting an interaction of ^{7}EFE^{9} of the N-terminus with the core.[36,45] This interaction is of importance when considering the R5L mutation's close proximity to the ^{7}EFE^{9} motif which may impact the formation or stability of fibers.[45] SFs and PHFs differ in their core conformations and fuzzy coat,[45] and tau filaments in different diseases form unique cross-sectional core conformations,[36,49–57] though most studies lack information on the N-terminus.[49–56] Additionally, various neuropathies have specific tau mutants or different ratios of isoforms that they are associated with.[49,50,58] Tau variants and mutants have shown differing aggregation propensities *in vitro*,[59] and likely impact their independent diseases.[57,60] Since these diseases also exhibit differences in tau folding *in vivo*,[49–56] there is a general hypothesis that these distinct folding tendencies lead to unique tauopathies.[55,57,60,61]

Tau aggregation does not occur *in vitro* unless at concentrations far higher than physiological conditions, even under pH and temperature extremes.[60,62,63] *In vitro,* tau aggregates in the presence of polyanions, which may reduce electrostatic repulsion between the highly charged tau molecules, thus lowering the energy barrier of aggregation.[40,60] Various polyanions have differing effects, for example SDS causes tau to form α-helices whereas arachidonic acid (ARA) makes tau form disease-relevant β-sheets.[60,64] ARA is richly found in neurons,[64] and its lipid peroxidation may be associated with the early phases of Alzheimer's disease, and precede the disease state.[64] Other polyanions have also been found to alter tau self-assembly and rate of polymerization, which may determine the structure of resultant filaments.[60]

The filament lengths of R5L and wild type tau have previously been studied using electron microscopy (EM). Interestingly, the EM studies on 2N4R R5L have found differing results. Whereas one study found that R5L produced shorter fibers than wild type,[17] a second study reported that it formed longer fibers.[29] While most studies of tau fiber morphologies have

used electron microscopy,[23,29,44] in the present work, atomic force microscopy (AFM) imaging was used to visualize tau fibers.[65,66] While both AFM and EM require that fibers are deposited on a substrate for imaging, AFM imaging does not require staining and has the flexibility to image fibers either dried on a surface or in fluid environments.[29,66]

Tau aggregation and its kinetics have also been monitored using both laser light scattering (LLS) and fluorimetry.[17,23,29] While LLS tends to yield more quantitative information about fiber density, it is limited in its ability to detect smaller fibers that are unable to scatter light at the wavelengths used in the measurements.[17] Fluorimetry is limited only by the fibers' ability to bind to the fluorescent dye and thus may be more sensitive to smaller fibers.[23] Similar to EM, comparative studies using scattering and fluorimetry have produced differing results for R5L versus WT aggregation, finding alternately that R5L increases,[17,29] decreases,[24] or does not affect[29] the amount of polymerization relative to WT, with results depending on the type of measurement or isoform studied.

Both AFM imaging and fluorimetry are used in this study to further understand the behavior of the R5L mutant and the different N-terminal isoforms of tau to better understand the role of the projection domain in aggregation. Since PD mutants such as R5L are found in specific diseases,[18] it is plausible that this mutation causes tau fibers to fold uniquely compared to WT.[55,60,61] Differences in tau fibers may show how the projection domain affects tau folding, especially in terms of its nucleation-elongation model. A better understanding of the role of the PD in aggregation and in filaments' fuzzy coat may elucidate of how various projection domain mutants and isoforms affect the progression of these diseases.[60]

2. Materials and Methods:

Cloning and Tau Purification:

2N4R tau (UniProt ID P10636) was obtained as previously described.[2] Mutagenesis to produce additional isoforms and mutants was performed using the Q5 Site Directed Mutagenesis Kit (New England Biolabs). 1N4R tau was generated using by an initial round of mutagenesis with primers (5'-CTGAAGAAGCAGGCATTGG-3' and 5'-CTTCCGCTGTTGGAGTGC-3') designed to eliminate one N-terminal insert (residues 74-103 in 2N4R tau), and 0N4R tau was generated with primers (5'-CTGAAGAAGCAGGCATTGGAG-3' and 5'-CTTTCAGGCCAGCGTCCG-3') that eliminated both N-terminal inserts (residues 45-103). The R5L mutation was added to each WT isoform using primers (5'-ATGTGACAGCACCCTTAGTG-3' and R: 5'-CTTTCAGGCCAGCGTCCG-3'). Template digestion and PCR product ligation were completed using the KLD Enzyme Mix standard protocol (New England Biolabs). The PCR products were transformed into DH5α competent cells and incubated overnight on LB-agar plates containing 100μM ampicillin. For each tau isoform, several single colonies were selected and plasmids purified using a QIAprep Spin Miniprep Kit (QIAGEN). DNA sequences confirmed with sequencing from Molecular Cloning Labs.

The mutated plasmids were transformed into One Shot BL21(DE3) Chemically Competent *E. coli* cells (Thermo Fisher) and incubated overnight at 37°C on LB-ampicillin plates. Tau purification was conducted as previously described,[2] with cells lysed using sonication on ice rather than French Press. Following the purification, tau concentrations were typically 0.1-0.5 mg/ml in BRB8 (8 mM K-Pipes, 0.1 mM EGTA, 0.1 mM $MgCl_2$, pH 6.8), and were lyophilized and stored at -20 ºC until use. Following purification, protein concentration was determined by micro-BCA assay with BSA as a standard.

Tau Aggregation

10mM arachidonic acid (ARA, Nuchek Prep) was aliquoted in ethanol and the solvent was blown off using nitrogen gas prior to storage at -80 ^{o}C. Lyophilized aliquots of tau were rehydrated with water to 1/10 of their original volume and then diluted to a final concentration at 5 μM or 10 μM in polymerization buffer (10 mM HEPES, 100 mM NaCl, 0.1 mM EDTA, 5 mM DTT, pH 7.64), with ARA in a 37.5:1 ratio to tau.[19] Polymers were allowed to grow for four days in darkness at room temperature.

AFM In-Air Imaging

30μL of polymerized tau sample was deposited onto freshly-cleaved muscovite mica (V-1 quality, Electron Microscopy Sciences) and adsorbed for 3 minutes. The sample was then rinsed with ~3mL water and dried using nitrogen gas. AFM imaging was conducted with a Bruker MultiMode AFM operating in intermittent contact mode, with POINTPROBE Silicon SPM Sensor cantilevers (42 N/m, NanoWorld).

Tau fibers for each image were individually selected, traced, and measured using a custom MATLAB script. The area covered by tau aggregates was determined after flattening and thresholding the image using a custom MATLAB script. We used a two-way ANOVA to analyze the effects of tau mutants and isoforms on fiber length. Fiber length data were log-transformed to normalize the data distributions. A post-hoc test was used to compare the effects of mutant vs WT on fiber length separately for each variant. Data analysis was conducted in R v4.3.3.[67]

Fluorescence Assay

After four days of polymerizing undisturbed in the dark, 1mM Thioflavin S (ThS, Sigma Aldrich) was added to each solution and measured using a Synergy HTX Multi-mode Microplate Reader (Biotek) using a 485/20nm excitation filter and 528/20nm emission filter.

3. Results:

3.1 R5L vs WT tau dry imaging

To define the terminology used in this paper, we use "fibers" or "fibrils" to describe isolated, well-structured polymers as observed in AFM images, "clusters" are groups of fibers that have accumulated to become indistinguishable with some fibril ends visible around the edges, and "aggregates" is inclusive of both fibers and clusters. AFM images were collected after four days of polymerization, which contrasts with other studies that only reported data on R5L up to 24 hours.[9,17,23,29] The density of protein observed in AFM images depends on the species' ability to bind uniformly to a well-defined surface (in this case mica), and the relative sample size is very small in comparison to the overall population, which results in some variability in the AFM images. To mitigate this, multiple images were taken of each sample in order to find representative areas of the surface.

Representative tau fibers for each isoform after four days of growth are depicted in Figure 3. Qualitatively, the images reveal the total amount of fibers on the surface and their tendency to cluster. The clustering phenomenon is mostly seen in 0N for both wild type and the mutant (clusters indicated by red arrows in Figure 3), although 1N was observed to cluster in some images.

For each isoform, at least three images were further analyzed to assess the amount of aggregation for each isoform. The following quantities were measured: the lengths of all fibers

in the images, the sum of the lengths of all fibers in the images, the number of fibers per image, and the percent area of the image covered by protein. Table 1 summarizes these quantitative data, and the distributions of fiber lengths are depicted in Figure 4. As shown in Table 1 and Figure 4, longer isoforms of tau formed longer fibers. Fiber length was significantly affected by mutant and isoform variant (two-way ANOVA, mutant: $F_{1, 1796} = 22.0$, $p < 0.001$, variant: $F_{2, 1796} = 140.2$, $p < 0.001$). There was also a significant interaction between mutant and isoform, such that differences between mutants were dependent on isoform (two-way ANOVA, $F_{2, 1796} = 3.2$, $p = 0.04$). When comparing mutant vs. WT, the mutation only significantly affected the average length of fibers for 0N4R tau ($p < 0.001$) and not 1N ($p = 0.07$) or 2N4R ($p = 0.70$).

The amount of tau aggregation in the AFM images was assessed in two separate ways. First, the total sum of the lengths for each image was measured and averaged (Table 1, Figure 5a). However, in images with many larger aggregates and clusters, it was difficult/impossible to distinguish and accurately measure each individual fiber, thus underestimating the total fiber density in those images. Therefore, as a second estimate of total tau polymerization, the total area of the surface covered by protein was measured and taken as a percentage of the image (Table 1, Figure 5b).

When only taking into consideration the distinguishable fibers (ie. the total length measurement, Figure 5a), 0N4R and 1N4R had similar amounts of fiber, whereas when considering total surface coverage, 0N4R aggregates more than 1N4R (Figure 5b). These data indicate that there is still the same amount of distinguishable fibers, and the extra area accumulated by 0N4R is clustered protein and is unassignable as individual fibers in our data.

Based on our data, the mutant had an opposite influence on total aggregation (Figures 5a and b) as compared to fiber length (Figure 4). Whereas the average length of 0N R5L fibers was

significantly longer than 0N WT (Figure 4), we observed that they form about the same total amount of aggregate (Figure 5a and b). When comparing WT vs. R5L, Both 1N and 2N tau form similar length fibers, yet for both isoforms R5L tau forms significantly more aggregates. In sum, we observed that the R5L mutation has a greater effect on the lengths of individual fibers of shorter isoforms, while the mutation produces more total aggregation for 1N and 2N4R and not 0N4R. These data are consistent with a previous report[19] that 1N4R aggregates around 50% more than 2N4R, and 0N4R tau has the highest total aggregation.

3.2 Results of fluorescence assay

Total tau aggregation was also measured using ThS fluorimetry after four days of growth (Figure 6). This assay showed similar results to AFM imaging when comparing mutants of the same isoform (Figure 5b). The fluorimetry results for 2N4R R5L are consistent with the trends observed in our AFM data, and with previous fluorimetry and LLS assays reporting that R5L increases the total aggregation for 2N tau.[17,29] For both the 1N and 0N isoforms, our fluorescence data indicate that R5L may aggregate slightly more that WT, which is consistent with our AFM total aggregation data, but differs from previously published data[23] on these shorter isoforms.

When comparing total fluorescence across isoforms, it is notable in our data that 1N R5L and WT produced the lowest total signal, with more total apparent aggregation from both 0N and 2N. These data contrast with previous reports that had observed a much smaller difference in total fluorescence across isoforms.[23] The trends in our fluorescence data across isoforms also differs slightly from our AFM data, where we observed that longer isoforms produced somewhat less total aggregation.

4. Discussion:

4.1 Comparison of AFM and Fluorometric Results

Discrepancies between AFM and fluorimetric data may be explained by contrasting the limitations and strengths of the two techniques. As previously mentioned, AFM imaging is limited by the ability of the protein and fibers to bind to the mica surface as well as the sample size being very small compared to the total population of fibers. In comparison, fluorescence may be able to detect very small fibers that are ThS-sensitive yet not visible at the resolution of our AFM images. The main caveat of the fluorimetry assay is that it depends on the interactions of ThS with filaments. ThS binds to PHFs more readily than SFs, and so it may be more sensitive to variants that favor PHFs over SFs,[68] conformations which we are unable to distinguish in our AFM imaging data, though this could be possible using higher resolution AFM or SEM.[44,66] Although R5L is a relatively small mutation, it is possible that ThS binding differs between the mutant and wild type tau, or between tau isoforms. In addition, ThS binds more readily to the middle portions of fibers than the ends, so it is more effective in measuring longer fibers.[69] This may explain why 2N tau has the highest fluorescence as compared to shorter isoforms, as it forms the longest fibers (Figures 3 and 6). ThS may also be excluded from the inner portions of large clusters of fibers as found for 0N and 1N tau, thus effectively reducing the relative measured fluorescence in those samples. In the future, a comparative study using Thioflavin T could further inform this study as it is a smaller molecule that may bind more effectively to all tau fibrils formed, and may be a more consistent reporter of tau polymerization.[68,70]

4.2 The Effect of Isoform on Tau Aggregation

Previous studies of R5L and WT tau isoforms have produced a varied picture of both isoform and mutant polymerization, and so it is important to place this study within the context of these reports. Some important factors to consider when comparing to earlier studies include the concentrations of tau and ARA, as well as the incubation times used for polymerization.

As previously reported, 0N tau has been found to undergo its nucleation step and form few elongated fibers, resulting in more globular filaments.[19,23,44] We have, on some occasions, observed that purification of 0N tau does not yield polymerization-competent protein, in spite of similar purity (assessed by SDS-PAGE), storage conditions, and age when compared to successful purifications (Supporting Information Figure 3). Yet, the fibers observed in Figure 4 for 0N4R WT and R5L contrasts previous reports that 0N tau will not fibrillize with ARA as an inducer.[23,44] As the presence of the N-terminal is inhibitory to aggregation,[30,42,43] a simple model would expect shorter N-terminal tau isoforms should be able to readily aggregate. Mutreja *et al*. reasoned that because their 0N tau formed large clusters of filaments, the fibers were unevenly distributed on their surface.[44]

Our data indicates that 0N tau has a higher tendency to accumulate and form clusters as compared to longer isoforms. This observation may be due to 0N forming the highest number of fibers, and indeed at higher concentrations we observed more clustering (Figure 3). Additionally, a higher propensity for clustering may be an inherent characteristic of 0N tau. A shorter projection domain results in a shorter fuzzy coat on fibrils, allowing more favorable interactions between fibers. With a smaller and less charged fuzzy coat, repulsion between fibers likely decreases and the negatively charged fuzzy coat can interact with the positively charged core. This is consistent with 1N and 2N showing minimal clustering whereas 0N has increased clustering.

Previous studies comparing 1N4R and 2N4R WT tau aggregation are summarized in Figure 7. Similarly to this study, others have found that 2N4R tau forms longer fibers than 1N4R.[19,23,44] However, they find different results in the total amount of aggregation for these two isoforms. Two of the studies, which used incubation times of overnight at 24 hours, found that

2N4R tau forms more fibers than 1N4R.[23,44] The same group also showed 1N4R forming around 50% more fibers than 2N4R, which used a concentration of 4 μM tau and an 8 hour incubation.[19] To add to these results, the present work found that 2N4R forms about 50% more fibers after four days at a concentration of 5 μM tau, with ratios of tau:ARA identical to previous studies. Taken together this work and previous work suggests that 2N4R has higher total aggregation under lower concentrations as compared to 1N4R, whereas 1N4R aggregates readily at higher concentrations. In the future, this can be further studied by systematically analyzing tau fibrils at different concentrations.

4.3 The Effect of the R5L Mutant on Tau Aggregation

Previous EM studies have also had varying results of fiber length and total aggregation for R5L versus wild type tau, some of which are summarized in Figure 8.[9,17,23,29] Of these studies, three only consider 2N4R tau. Combs and Gamblin found in 2012 that 2N4R R5L tau forms longer fibers with the same amount of total aggregate after incubating overnight.[29] However, in 2019, the same lab reported that 2N4R R5L has the same length and total aggregation as wild type under the exact same conditions.[23] Additionally, in 2003, Gamblin *et al.* found that 2N4R R5L forms shorter fibers, about half the length of wild type, and that R5L forms more total aggregate compared to WT. However, that study used half the ratio of arachidonic acid:tau and only polymerized the protein for five hours.[17] Using the aggregation inducer thiazine red rather than ARA, Chang *et al*. found that after 24 hours all concentrations of tau ranging from 0.2 μM to 0.8 μM show 2N4R R5L forms the same length fibers as wild type, however R5L forms more total aggregate.[9] The results reported herein are most consistent with the study by Chang *et al*.[9]

A previous study using all three N-terminal isoforms of 4R tau similarly agrees with part of the conclusions from this experiment.[23] Although this previous work found that 0N tau did not form elongated fibers, they did find that 0N R5L formed fewer total aggregates than WT and fibers were shorter in length. For the 1N isoform, the previous study found that the R5L mutation did not affect either the total aggregation or length of filaments,[23] whereas our work observes the mutation increasing the aggregate mass. We note that there are differences in the conditions used by Mutreja *et al.* and those used here, as we used 5 μM tau concentration and a 5 day incubation, while Mutreja *et al*. used a concentration of 2 μM and overnight incubation.[23]

4.4 The Role of the Projection Domain in Tau's Nucleation-Elongation Pathway

Based on our combined AFM and fluorimetry results, the R5L mutation increases the length of 0N4R fibers while not affecting its total amount of aggregation. In contrast, for the 1N and 2N isoforms, the R5L mutation does not alter fiber length yet increases the total amount of aggregation. Since R5L forms more fibers for both 1N and 2N, however of the same length as WT, we hypothesize that the mutation only affects the nucleation step of tau's aggregation pathway for longer isoforms. Similarly, only the fibril length of 0N tau is affected by the R5L mutation while forming the same total amount of fibrils, suggesting that the mutation alters the elongation process of fibrillization for the shorter 0N isoform. Therefore, the data presented herein may indicate that the R5L mutation more strongly impacts the nucleation of longer isoforms and the elongation of shorter isoforms.

Based on the data presented here, the N-terminal deletions (between 2N, 1N and 0N) likely play the biggest role in altering the nucleation steps of tau, with the R5L mutation having a smaller impact on nucleation. Because the N-terminus inhibits aggregation,[34,71] it is not surprising that the shorter isoforms could permit a greater total amount of aggregation.[43] We

hypothesize that the decrease in negative charge in the projection domain region as found in 0N4R and 1N4R tau may cause polymerization-resistant secondary structures such as the paperclip conformation to be less stable, therefore leading to more nucleation followed by aggregation.[9] When comparing WT to R5L, the mutation of one basic residue has a minimal impact on the paperclip conformation relative to the removal of the N-terminal repeats, therefore making any differences in nucleation statistically insignificant in our measurements. Whereas for the 2N4R isoform, the R5L mutation appears to have a greater destabilizing effect on the paperclip conformation and/or other transient secondary structures.[34] Destabilization of polymerization-resistant conformations by the R5L mutation[29] would bias the protein towards unfolding and nucleation, which would result more total aggregation as observed here and by others.[9,32,35] This is consistent with earlier work by Chang *et al.*, who found that 2N4R R5L has an increased nucleation rate but no change in elongation.[9]

The data presented herein show that isoforms with longer projection domains form longer fibers, and we hypothesize that there are two complementary effects that contribute to this behavior. Previous work with cryo-EM found that there are stabilizing interactions between the negatively-charged projection domain and the positively-charged filament core, with the ^{7}EFE^{9} motif participating in a key interaction.[45] Thus, the higher negative charge density of the projection domain in longer isoforms may result in more favorable electrostatic interactions with the filament core, resulting in the formation of longer fibers. For a similar reason, we posit that the R5L mutation, in close proximity to the ^{7}EFE^{9} motif,[18,45] would also have a stabilizing effect that favors longer fibers. In our data, the specific stabilization caused by the R5L mutation does not lead to statistically significant changes in fiber length for the 1N or 2N isoforms, but does so

for the 0N isoform. This may be due to the greater relative effect of a single mutation on the acidity of this region in the shorter projection domain.

Future studies including multiple days of AFM imaging combined with time-based fluorimetry measurements could yield additional insights into the kinetics of tau aggregation. As previously mentioned, the smaller fluorescent dye Thioflavin T binds more readily to tau fibers,[68] and can be used to study kinetics.[60,70] In addition, by using AFM images to study the aggregation of tau over time, it may be determined whether either the primary or secondary nucleation step determines the rate of aggregation.[32] This work used 5μM tau concentration during polymerization, which is similar to intracellular tau concentrations of 2-4μM,[19] however using smaller concentrations of tau can help to better compare to previous reports.[9,23,44] [10,24,48] To form filaments closer to those found in disease, recent work has reported variations in tau fiber structures using different polyanion inducers.[60] By using these techniques to form aggregates similar to those collected *in vivo*, the information gathered by *in vitro* experiments may be more disease-relevant. Similarly, to differentiate these filaments, conducting AFM imaging in liquid environments may help better understand the hydrated fiber structure, how tau fibers interact, and whether PHFs or SFs are formed by specific tau variants.[34,66]

5. Conclusions:

The projection domain was observed to significantly impact the formation of tau aggregates. Shorter isoforms of tau formed the greatest number of aggregates, yet longer isoforms formed longer fibers. Using the R5L mutation as a lens to study the PD, we hypothesize that the mutation affected the nucleation of longer isoforms due to its impact on tau's transient structure in solution and elongation of shorter isoforms by impacting the interactions between the PD and the filament core.

A better understanding of the pathways of aggregate formation is essential for future inhibitive drug designs.[58] For example, they could focus on tau nucleates, or seeds, that are known to be able to spread throughout the brain and infect other regions of the brain.[58] This study provides evidence that shorter projection domain isoforms have a greater aggregation propensity and form the most amount of seeds, though aggregation propensity does not seem to correlate with higher seed spreading.[72] Previous studies have shown various diseases having different ratios of 3R:4R tau,[4,5] and perhaps ratios of 0N:1N:2N tau are also important. Further study into other PD mutants such as R5H may further elucidate the importance of the projection domain in aggregation as found in this study.[21]

Acknowledgements:

This work was made possible by the NIH grant #1R15N5108245-01A1 and the Vassar College Undergraduate Research Summer Institute (URSI) program. Thank you to Shira Freilich, Shaharia Khan, and Lukas Johnson for providing some of the purified proteins used in this study.

Supporting Information:

AFM images annotated with traced fiber lengths, AFM images with protein area assignments highlighted, and AFM images comparing successful and unsuccessful purifications of 0N4R tau.

References

1. Chang, C.-W., Shao, E. & Mucke, L. Tau: Enabler of diverse brain disorders and target of rapidly evolving therapeutic strategies. *Science* **371**, (2021).
2. Donhauser, Z. J., Saunders, J. T., D'Urso, D. S. & Garrett, T. A. Dimerization and Long-Range Repulsion Established by Both Termini of the Microtubule-Associated Protein Tau. *Biochemistry* **56**, 5900–5909 (2017).

3. Barbier, P. *et al.* Role of Tau as a Microtubule-Associated Protein: Structural and Functional Aspects. *Front. Aging Neurosci.* **11:204**, (2019).
4. Hernandez, F. *et al.* Tau Aggregation. *Neuroscience* **518**, 64–69 (2023).
5. Goedert, M. & Spillantini, M. G. Ordered Assembly of Tau Protein and Neurodegeneration. in *Tau Biology* (eds. Takashima, A., Wolozin, B. & Buee, L.) vol. 1184 3–21 (Springer Singapore, Singapore, 2019).
6. Combs, B., Voss, K. & Gamblin, T. C. Pseudohyperphosphorylation Has Differential Effects on Polymerization and Function of Tau Isoforms. *Biochemistry* **50**, 9446–9456 (2011).
7. Mukhopadhyay, R. & Hoh, J. H. AFM force measurements on microtubule-associated proteins: the projection domain exerts a long-range repulsive force. *FEBS Lett.* **505**, 374–378 (2001).
8. Majewski, J. *et al.* Lipid membrane templated misfolding and self-assembly of intrinsically disordered tau protein. *Sci. Rep. Nat. Res.* **10**, (2020).
9. Chang, E., Kim, S., Yin, H., Nagaraja, H. N. & Kuret, J. Pathogenic missense MAPT mutations differentially modulate tau aggregation propensity at nucleation and extension steps. *J. Neurochem.* **107**, 1113–1123 (2008).
10. Strang, K. H., Golde, T. E. & Giasson, B. I. MAPT mutations, tauopathy, and mechanisms of neurodegeneration. *Lab. Invest.* **99**, 912–928 (2019).
11. Kondo, J. *et al.* The Carboxyl Third of Tau Is Tightly Bound to Paired Helical Filaments. *Neuron* **1**, 827–834 (1988).
12. Gray, E. G., Paula-Barbosa, M. & Roher, A. Alzheimer's Disease: Paired Helical Filaments and Cytomembranes. *Neuropathol. Appl. Neurobiol.* **13**, 91–110 (1987).
13. Kellogg, E. H. *et al.* Near-atomic model of microtubule-tau interactions. *Sci. Struct. Biol.* **360**, 1242–1246 (2018).
14. Rosenberg, K. J., Ross, J. L., Feinstein, H. E., Feinstein, S. C. & Israelachvili, J. Complementary dimerization of microtubule-associated tau protein: Implications for microtubule bundling and tau-mediated pathogenesis. *Proc. Natl. Acad. Sci.* **105**, 7445–7450 (2008).

15. Cario, A. *et al.* The pathogenic R5L mutation disrupts formation of Tau complexes on the microtubule by altering local N-terminal structure. *Proc. Natl. Acad. Sci. U. S. A.* **119**, (2022).
16. Jeganathan, S., Von Bergen, M., Mandelkow, E.-M. & Mandelkow, E. The Natively Unfolded Character of Tau and Its Aggregation to Alzheimer-like Paired Helical Filaments. *ACS Biochem.* **47**, 10526–10539 (2008).
17. Gamblin, T. C., Berry, R. W. & Binder, L. I. Tau Polymerization: Role of the Amino Terminus. *ACS Biochem.* **42**, 2252–2257 (2003).
18. Poorkaj, P. *et al.* An R5L tau mutation in a subject with a progressive supranuclear palsy phenotype. *Ann. Neurol.* **52**, 511–516 (2002).
19. King, M. E., Gamblin, T. C., Kuret, J. & Binder, L. I. Differential assembly of human tau isoforms in the presence of arachidonic acid. *J. Neurochem.* **74**, 1749–1757 (2000).
20. Combs, B., Hamel, C. & Kanaan, N. M. Pathological conformations involving the amino terminus of tau occur early in Alzheimer's disease and are differentially detected by monoclonal antibodies. *Neurobiol. Dis.* **94**, 18–31 (2016).
21. Hayashi, S. *et al.* Late-onset frontotemporal dementia with a novel exon 1 (Arg5His) tau gene mutation. *Ann. Neurol.* **51**, 525–530 (2002).
22. Ghetti, B., Wszolek, Z. K., Boeve, B. F., Spina, S. & Goedert, M. Frontotemporal Dementia and Parkinsonism Linked to Chromosome 17. *Folia Neuropathol.* **43**, 258–270 (2005).
23. Mutreja, Y., Combs, B. & Gamblin, T. C. FTDP-17 Mutations Alter the Aggregation and Microtubule Stabilization Propensity of Tau in an Isoform-Specific Fashion. *ACS Biochem.* **58**, 742–754 (2019).
24. Cario, A., Wickramasinghe, S. P., Rhoades, E. & Berger, C. L. The N-terminal disease–associated R5L Tau mutation increases microtubule shrinkage rate due to disruption of microtubule-bound Tau patches. *J. Biol. Chem.* **298**, (2022).
25. Jeganathan, S., Von Bergen, M., Brutlach, H., Steinhoff, H.-J. & Mandelkow, E. Global Hairpin Folding of Tau in Solution. *ACS Biochem.* **45**, 2283–2293 (2006).

26. Mukrasch, M. D. *et al.* Structural Polymorphism of 441-Residue Tau at Single Residue Resolution. *PLOS Biol.* **7**, (2009).

27. Jeganathan, S. *et al.* Proline-directed pseudo-phosphorylation at AT8 and PHF1 epitopes induces a compaction of the paperclip folding of Tau and generates a pathological (MC-1) conformation. *J. Biol. Chem.* **283**, 32066–32076 (2008).

28. Jeganathan, S., Chinnathambi, S., Mandelkow, E.-M. & Mandelkow, E. Conformations of Microtubule-Associated Protein Tau Mapped by Fluorescence Resonance Energy Transfer. in *Amyloid Proteins: Methods and Protocols* (eds. Sigurdsson, E. M., Calero, M. & Gasset, M.) vol. 849 85–99 (Humana Press, Totowa, NJ, 2012).

29. Combs, B. & Gamblin, T. C. FTDP-17 Tau Mutations Induce Distinct Effects on Aggregation and Microtubule Interactions. *Biochemistry* **51**, 8597–8607 (2012).

30. Pounot, K. *et al.* Mutations in Tau Protein Promote Aggregation by Favoring Extended Conformations. *JACS Au* **4**, 92–100 (2024).

31. Carmel, G., Mager, E. M., Binder, L. I. & Kuret, J. The Structural Basis of Monoclonal Antibody Alz50's Selectivity for Alzheimer's Disease Pathology. *J. Biol. Chem.* **271**, 32789–32795 (1996).

32. Lövestam, S. *et al.* Disease-specific tau filaments assemble via polymorphic intermediates. *Nature* **625**, 119–125 (2024).

33. Elbaum-Garfinkle, S. & Rhoades, E. Identification of an Aggregation-Prone Structure of Tau. *J. Am. Chem. Soc.* **134**, 16607–16613 (2012).

34. Wegmann, S., Schöler, J., Bippes, C. A., Mandelkow, E. & Muller, D. J. Competing Interactions Stabilize Pro- and Anti-aggregant Conformations of Human Tau. *J. Biol. Chem.* **286**, 20512–20524 (2011).

35. Congdon, E. E. *et al.* Nucleation-dependent Tau Filament Formation. *J. Biol. Chem.* **283**, 13806–13816 (2008).

36. Falcon, B. *et al.* Tau filaments from multiple cases of sporadic and inherited Alzheimer's disease adopt a common fold. *Acta Neuropathol. (Berl.)* **136**, 699–708 (2018).

37. Fernandez-Ramirez, M. del C., Ng, K. K., Menéndez, M. & Laurents, Douglas V. Expanded Conformations of Monomeric Tau Initiate Its Amyloidogenesis. *Angew. Chem. Int. Ed.* **62**, (2023).

38. Necula, M. & Kuret, J. Site-specific pseudophosphorylation modulates the rate of tau filament dissociation. *FEBS Lett.* **579**, 1453–1457 (2005).

39. Kumar, H. & Udgaonkar, J. B. Mechanistic and Structural Origins of the Asymmetric Barrier to Prion-like Cross-Seeding between Tau-3R and Tau-4R. *J. Mol. Biol.* **430**, 5304–5312 (2018).

40. Carlson, S. W. *et al.* A Complex Mechanism for Inducer Mediated Tau Polymerization. *Biochemistry* **46**, 8838–8849 (2007).

41. Kumar, H. & Udgaonkar, J. B. Mechanistic approaches to understand the prion-like propagation of aggregates of the human tau protein. *Biochim. Biophys. Acta BBA - Proteins Proteomics* **1867**, 922–932 (2019).

42. El Mammeri, N., Duan, P., Dregni, A. J. & Hong, M. Amyloid fibril structures of tau: Conformational plasticity of the second microtubule-binding repeat. *Sci. Adv.* **9**, (2023).

43. Moore, C. L. *et al.* Secondary Nucleating Sequences Affect Kinetics and Thermodynamics of Tau Aggregation. *ACS Biochem.* **50**, 10876–10886 (2011).

44. Mutreja, Y. & Gamblin, T. C. Optimization of in vitro conditions to study the arachidonic acid induction of 4R isoforms of the microtubule-associated protein tau. in *Methods in Cell Biology* vol. 141 65–88 (Elsevier, 2017).

45. Fitzpatrick, A. W. P. *et al.* Cryo-EM structures of tau filaments from Alzheimer's disease. *Nature* **547**, 185–190 (2017).

46. Wischik, C. M. *et al.* Isolation of a fragment of tau derived from the core of the paired helical filament of Alzheimer disease. *Proc. Natl. Acad. Sci.* **85**, 4506–4510 (1988).

47. Novak, M., Kabat, J. & Wischik, C. M. Molecular characterization of the minimal protease resistant tau unit of the Alzheimer's disease paired helical filament. *EMBO J.* **12**, 365–370 (1993).

48. Duan, P., El Mammeri, N. & Hong, M. Milligram-scale assembly and NMR fingerprint of tau fibrils adopting the Alzheimer's disease fold. *J. Biol. Chem.* **300**, 107326 (2024).

49. Shi, Y. *et al.* Structure-based classification of tauopathies. *Nature* **598**, 359–363 (2021).

50. Zhang, W. *et al.* Novel tau filament fold in corticobasal degeneration. *Nature* **580**, 283–287 (2020).

51. Zhang, W. *et al.* Heparin-induced tau filaments are polymorphic and differ from those in Alzheimer's and Pick's diseases. *eLife* **8**, (2019).

52. Tarutani, A. *et al.* Cryo-EM structures of tau filaments from SH-SY5Y cells seeded with brain extracts from cases of Alzheimer's disease and corticobasal degeneration. *FEBS Open Bio* **13**, 1394–1404 (2023).

53. Shi, Y., Ghetti, B., Goedert, M. & Scheres, S. H. W. Cryo-EM Structures of Chronic Traumatic Encephalopathy Tau Filaments with PET Ligand Flortaucipir. *J. Mol. Biol.* **435**, (2023).

54. Lövestam, S. & Scheres, S. H. W. High-throughput cryo-EM structure determination of amyloids. *Faraday Discuss.* **240**, 243–260 (2022).

55. Falcon, B. *et al.* Novel tau filament fold in chronic traumatic encephalopathy encloses hydrophobic molecules. *Nature* **568**, 420–423 (2019).

56. Lövestam, S. *et al.* Assembly of recombinant tau into filaments identical to those of Alzheimer's disease and chronic traumatic encephalopathy. *eLife* **11**, (2022).

57. Lutter, L. *et al.* Structural Identification of Individual Helical Amyloid Filaments by Integration of Cryo-Electron Microscopy-Derived Maps in Comparative Morphometric Atomic Force Microscopy Image Analysis. *J. Mol. Biol.* **434**, (2022).

58. Scheres, S. H. W., Ryskeldi-Falcon, B. & Goedert, M. Molecular pathology of neurodegenerative diseases by cryo-EM of amyloids. *Nature* **621**, 701–710 (2023).

59. Munari, F., D'Onofrio, M. & Assfalg, M. Solution NMR insights into dynamic supramolecular assemblies of disordered amyloidogenic proteins. *Arch. Biochem. Biophys.* **683**, (2020).

60. Montgomery, K. M. *et al.* Chemical Features of Polyanions Modulate Tau Aggregation and Conformational States. *J. Am. Chem. Soc.* **145**, 3926–3936 (2023).

61. Kovacs, G. G., Ghetti, B. & Goedert, M. Classification of diseases with accumulation of Tau protein. *Neuropathol. Appl. Neurobiol.* **48**, (2022).

62. Kuret, J. *et al.* Pathways of tau fibrillization. *Biochim. Biophys. Acta BBA - Mol. Basis Dis.* **1739**, 167–178 (2005).

63. Shkumatov, A. V., Chinnathambi, S., Mandelkow, E. & Svergun, D. I. Structural memory of natively unfolded tau protein detected by small-angle X-ray scattering. *Proteins Struct. Funct. Bioinforma.* **79**, 2122–2131 (2011).

64. Barracchia, C. G. *et al.* Unsaturated Fatty Acid-Induced Conformational Transitions and Aggregation of the Repeat Domain of Tau. *Molecules* **25**, (2020).

65. Orasanu-Gourlay, A. & Bradley, R. H. Protein Adsorption by Basal Plane Graphite Surfaces: Molecular Images and Nano-Structured Films. *Adsorpt. Sci. Technol.* **24**, 117–130 (2006).

66. Wegmann, S., Medalsy, I. D., Mandelkow, E. & Müller, D. J. The fuzzy coat of pathological human Tau fibrils is a two-layered polyelectrolyte brush. *Proc. Natl. Acad. Sci.* **110**, (2013).

67. R Core Team. R: A Language and Environment for Statistical Computing. R Foundation for Statistical Computing. Vienna, Austria (2024).

68. Lakatoš, B., Kaliňaková, B., Hudecová, D. & Varečka, Ľ. New effects and applications of thioflavins. *Open Life Sci.* **5**, 143–150 (2010).

69. Santa-María, I., Pérez, M., Hernández, F., Avila, J. & Moreno, F. J. Characteristics of the binding of thioflavin S to tau paired helical filaments. *J. Alzheimers Dis.* **9**, 279–285 (2006).

70. Friedhoff, P., Schneider, A., Mandelkow, E.-M. & Mandelkow, E. Rapid Assembly of Alzheimer-like Paired Helical Filaments from Microtubule-Associated Protein Tau Monitored by Fluorescence in Solution. *Biochemistry* **37**, 10223–10230 (1998).

71. Von Bergen, M. *et al.* The Core of Tau-Paired Helical Filaments Studied by Scanning Transmission Electron Microscopy and Limited Proteolysis. *ACS Biochem.* **45**, 6446–6457 (2006).

72. Rodrigues, S. *et al.* Spreading of Tau Protein Does Not Depend on Aggregation Propensity. *J. Mol. Neurosci.* **73**, 693–712 (2023).

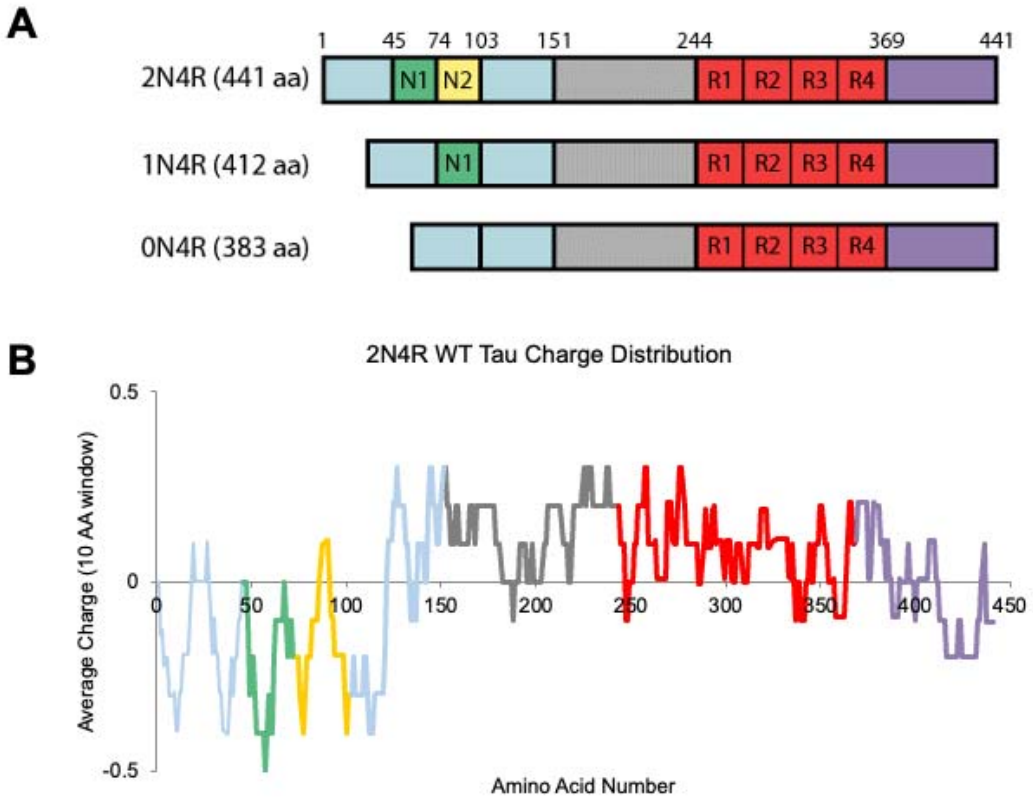

Figure 1: a) Structures of 2N, 1N, and 0N4R wild type tau, which consist of the projection domain (blue, with the N1 (green) and N2 (yellow) inserts labeled), proline-rich region (grey), microtubule binding region (red), and C-terminus (purple). Each isoform varies in its number of N-terminal repeats. b) The charge distribution of 2N4R wild type tau at pH 7.2, with charge averaged over a 10-residue window. In 1N4R the N2 (yellow) portion is eliminated, and in 0N4R both the N1 (green) and N2 (yellow) repeats are eliminated. The projection domain and C-terminal are negatively charged, whereas the proline-rich region and the MTBD are positively charged. In shorter isoforms, the projection domain has a lower charge density owing to the loss of acidic residues in the N-terminal inserts.

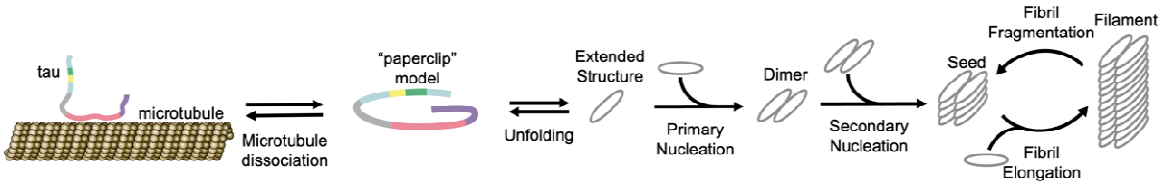

Figure 2: Nucleation-elongation reaction of tau into fibers. When tau dissociates from the microtubule and forms one of its secondary structures (paperclip shown in this figure), it can either reassociate or conformationally change in order to nucleate and then elongate into paired helical filaments or straight filaments.[9,16,41]

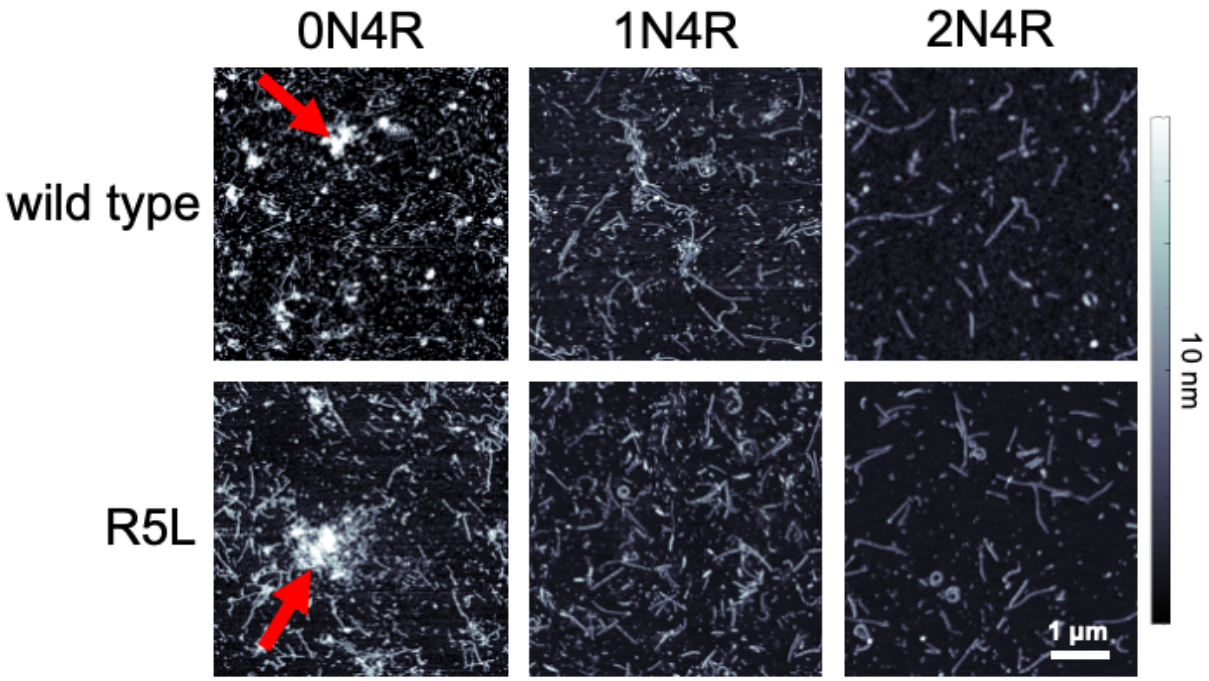

Figure 3: AFM in-air images of all tau fibers analyzed after four days of polymerization on mica at 5μM. The red arrows indicate two examples of tau clusters.

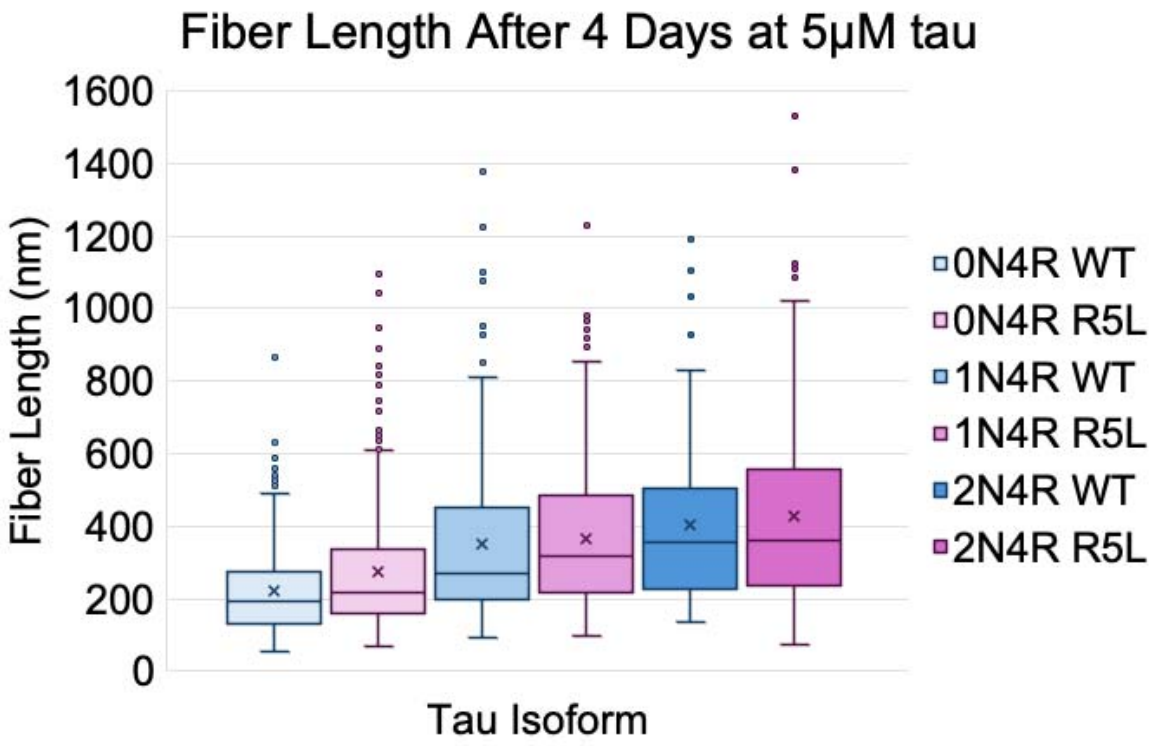

Figure 4: Fiber length of each tau variant studied after four days of growth at 5μM. The fiber lengths were gathered by selecting distinguishable fibers on three different 5μm AFM images. X represents the sample mean.

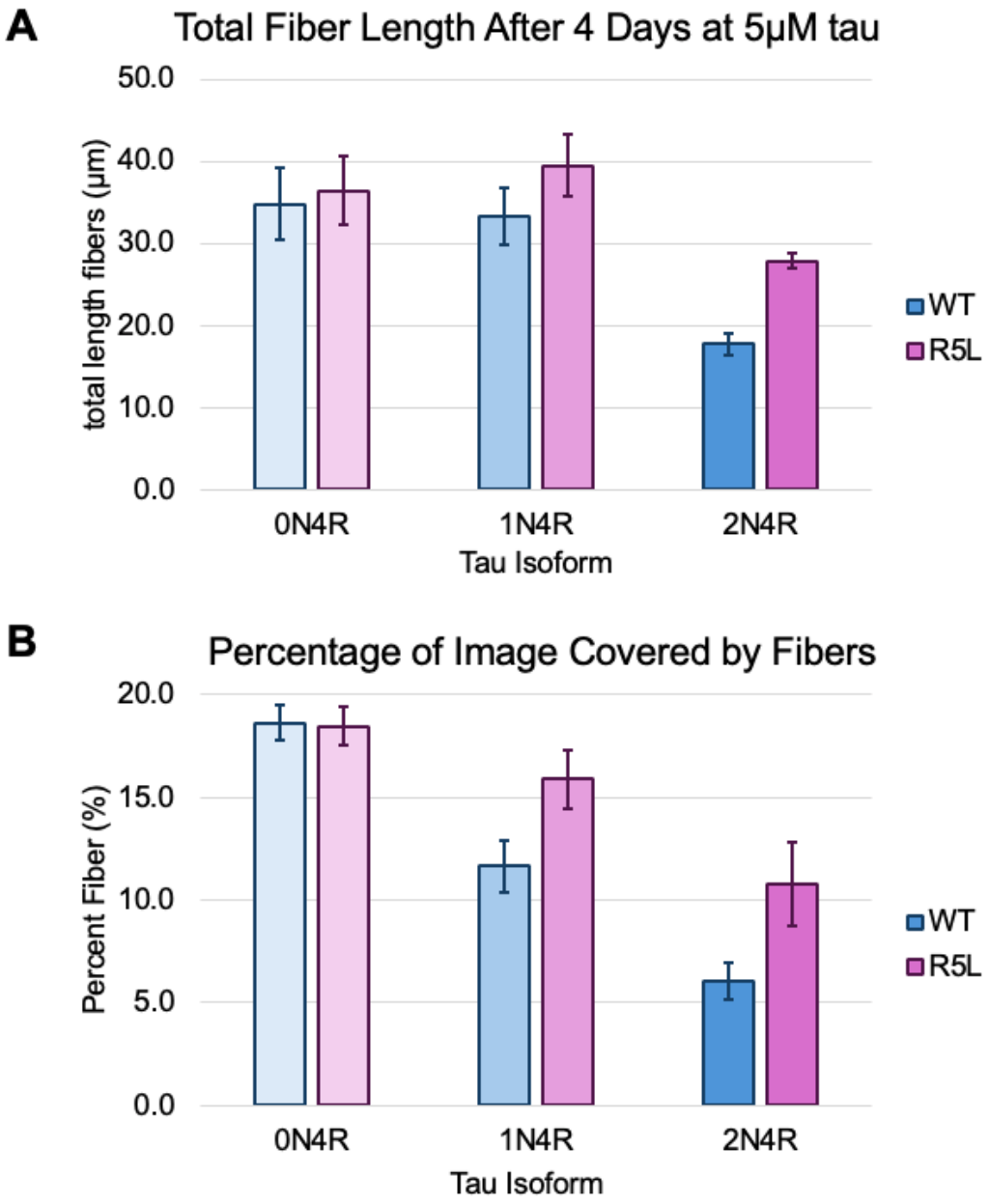

Figure 5: a) The total length of tau fibers for each variant after four days at 5μM. The total length of fibers per 5μm image was calculated along with its standard deviation. b) The percentage of the image covered by each tau variant's aggregates after four days at 5μM. The total area covered by tau aggregates was determined for each 5μm image and normalized to the total area of the image, which was done for three images.

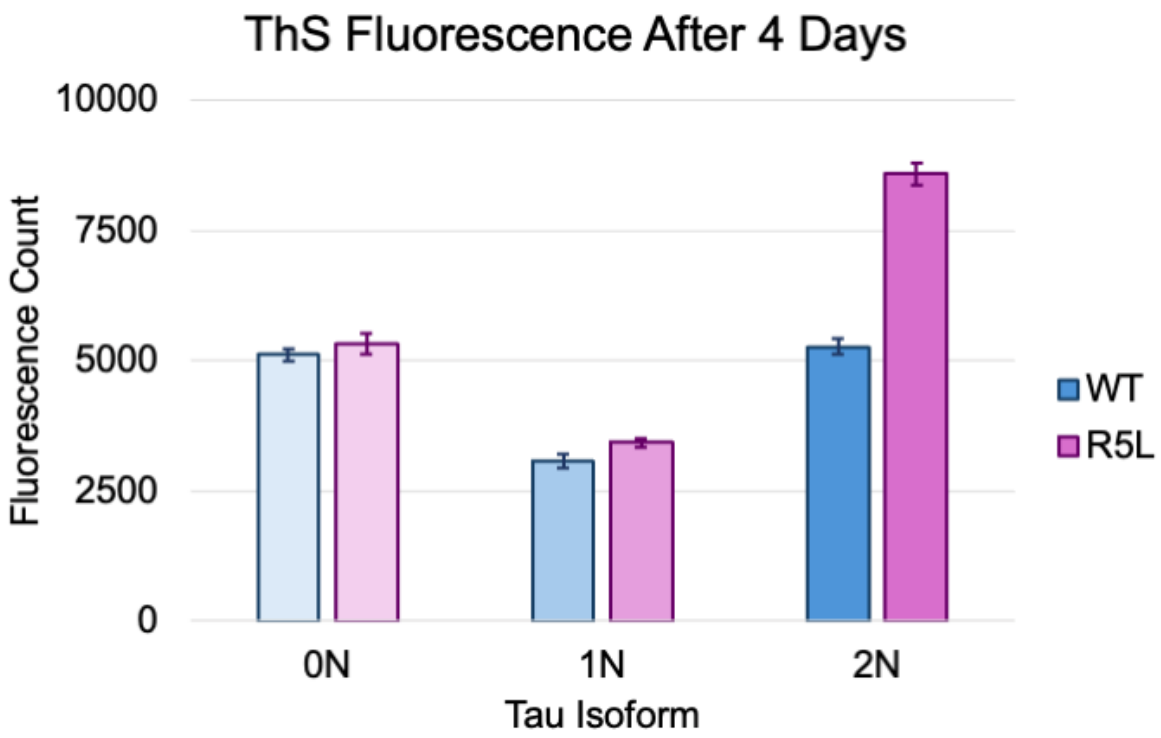

Figure 6: The total ThS fluorescence for all tau variants after 4 days at 5μM. Each bar represents an average of three measurements.

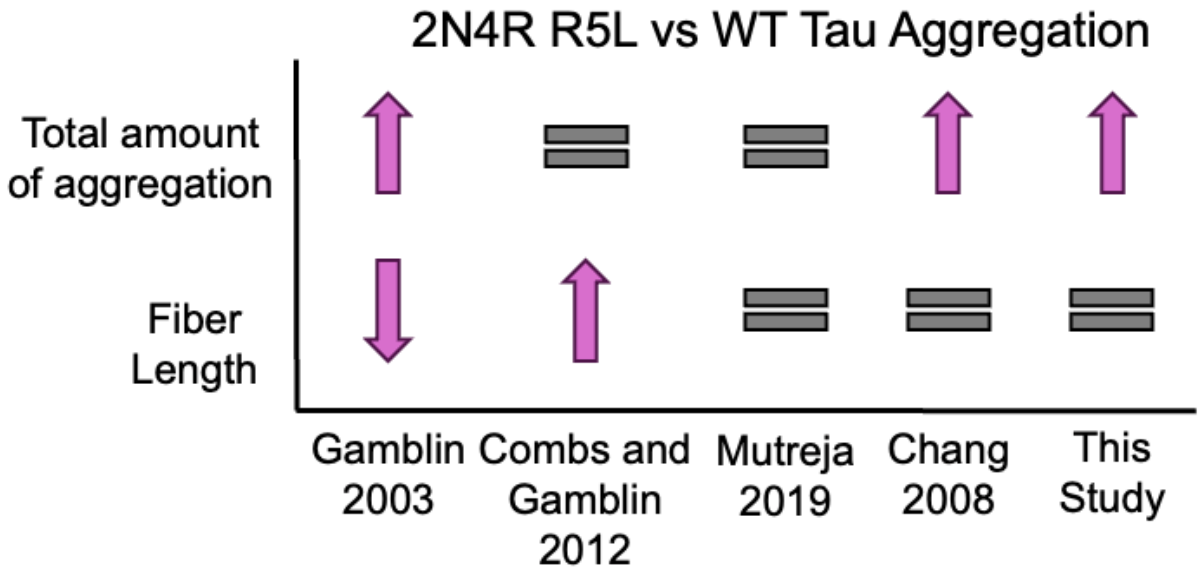

Figure 7: Previous results for 1N vs 2N4R tau alongside the results from this study. Arrows are in terms of 2N4R tau, where an upwards arrow means more aggregation/longer fibers for 2N, downwards arrows indicate less aggregation/shorter fibers for 2N tau.

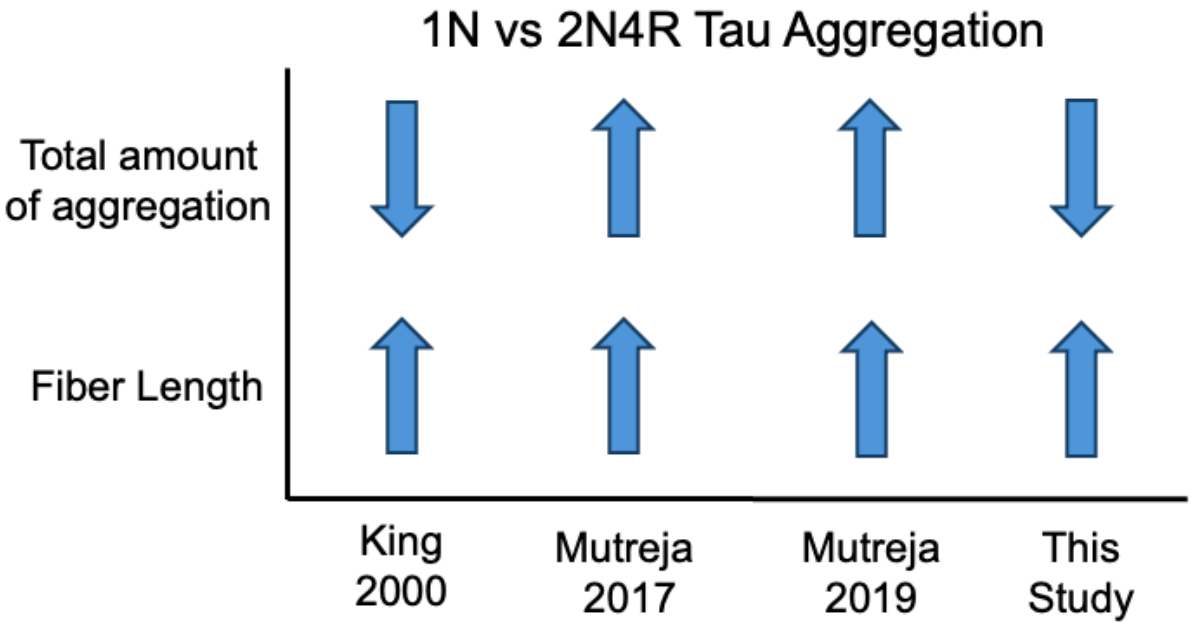

Figure 8: Previous results for 2N4R R5L vs WT tau alongside the results from this study. Arrows are in terms of R5L tau, where an upwards arrow means more aggregation/longer fibers for R5L, downwards arrows indicate less aggregation/shorter fibers for R5L tau, and an equals sign indicates that the aggregation/length is similar for R5L and WT.